Therefore, a mesh size enough to obtain an accurate field solution was advisable so, the minimum length of each edge of tetrahedra in the structure was 0.2 cm. The solution was performed at a single frequency of 900 MHz.

Agilent HFSS imposes boundary conditions at all surfaces exposed to the edge of the meshed problem region. This includes all outer surfaces and all surfaces exposed to voids and surface discontinuities within the structure. The radiation boundary condition, which encloses the whole structure, was selected in our problem. Radiation boundary models surfaces that represent open surfaces. Energy is allowed to radiate from these boundaries instead of being contained within them; waves can radiate out of the structure and toward the radiation boundary. The system absorbs the wave at the radiation boundary, essentially ballooning the boundary infinitely far away from the structure and into the space. The tangential component of E-field was solved by the program. In our problem, the radiation boundary was a cube with the length of 23 cm. The material was assigned to the radiation boundary as air.

It was possible to view and analyze electric field by the post processor of the program

SIMULATION RESULTS

The first, the human head was modeled in single layer with a dipole antenna. The electric-field distribution in the head and the SAR values in the head were illustrated in figure 2.

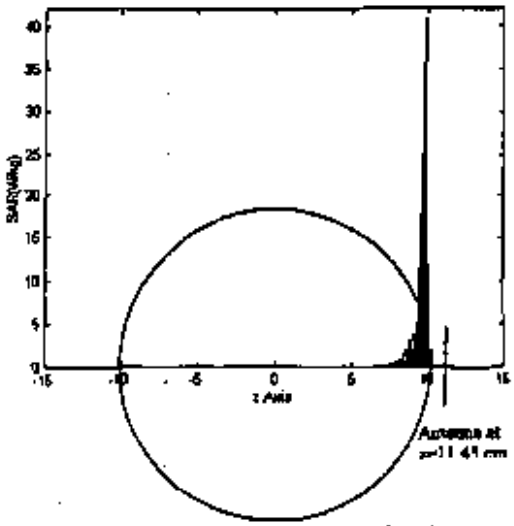

Figure 2. The distribution of local SAR values in the yz-plane for single-layered human head model

The peak value of the local SAR was found as 40.7296 W/kg Secondly, the single sphere with diameter of 1.8 was assumed pure brain (Table 2 [10]) just like the human head. The dipole antenna was located on z=2cm. The antenna and the rat model were in a radiation boundary, which was modeled as a cube with the length of 2.3 cm.

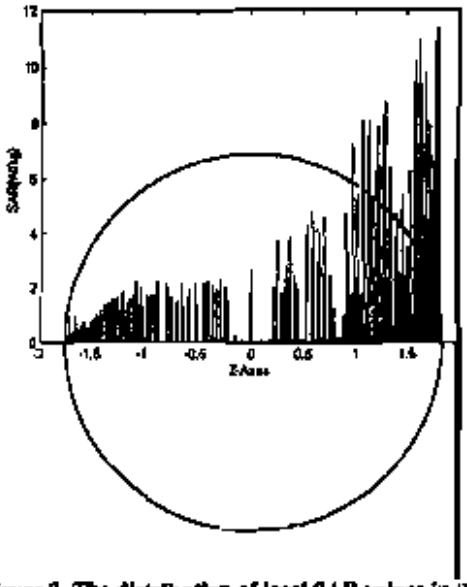

Figure 3. The distribution of local SAR values in the yz-plane for single rat head model

The peak value of local SAR in the three-layered spherical rat modeling was found as 11.3766 W/kg.

Thirdly, three concentric spheres with diameters of 1.8, 1.55, and 1.5 cm were used for modeling of the rat head

The relative permittivity ε', conductivity σ, and density ρ used in simulation were given in Table 2.

Table 2. The tissues and the properties used in simulations for rat

Layer	Tissue Model ed	Thickness (cm)	Relative Permittivity ε,	Conductivity σ (mΩ^-1/m)	Density ρ (kg/m³)	Loss Tangent (ε''/ε')
1	Brain	1.5	55	1	1050	0.363
2	Bone	0.05	3.5	0.15	1990	0.6
3	Skin	0.25	45	0.76	1040	0.337

The distribution of the local SAR values in the yz-plane were given in figure 4:

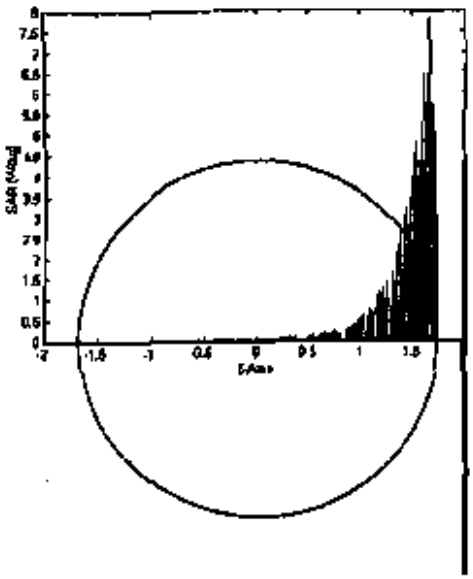

Figure 4. The distribution of local SAR values in the yz-plane for three-layered rat head model

The peak value of local SAR in the three-layered spherical rat modeling was found as 7.6919 W/kg.

THE COMPARISON OF THE RESULTS WITH THE LITERATURE

The comparisons of the peak values of local SAR with some of the previous studies were given below for human head models and rat head models. But the first comparison is made for radiation pattern as seen figure 5 and excellent agreement was obtained.

The Comparison of the Human Head Models

In the study of Konstantina S. Nikita a dipole antenna was used and the antenna input power was 1W. The dyadic Green's function was used for computation of the problem. The parameters used in simulations in our study were taken from this study in order to be able to compare the results.
The local peak SAR values in Nikita's study [3] and in our study were given in table 3. The difference between two studies is as follows:

Table 3. Comparison of the Peak SAR Values

	Homogeneous Sphere
Peak Values of Local SAR (W/kg) of Nikita's Study [3]	39.4
Peak Value of local SAR of Our Study	40.7296
Difference (%)	3.26

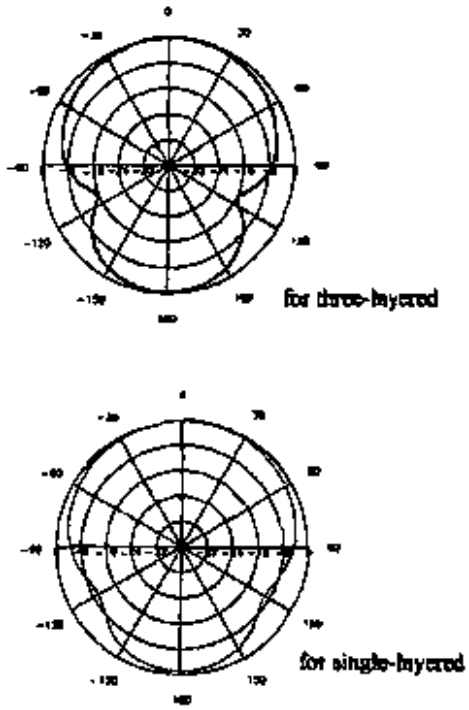

Figure 5. Radiation patterns for human head obtained in our study (vertical cut, 180°).

The Comparison of the Rat Models

The results of the rat-head modeling were compared with the results of in vivo tests, which were conducted on the rats at Istanbul University, Cerrahpasa Faculty of Medicine [11].

Table 4. Comparison of the Peak Values of Local SAR

		Peak Values of Local SAR (W/kg)
In vivo tests (51.5 V/m) [11]		6.732
Our Study	single-layered	11.3766
	three-layered	7.691

It can be seen from above comparison that there is a good agreement between the patterns and the local SAR values of our study with the literature.
The difference in table 3 and 4 can be easily reduced to lower level if we change some of the biological parameters.

CONCLUSION

In this study, spherical human head and dipole antenna were modeled to investigate the effects of the electromagnetic field of an antenna on human head because of the impossibility of the in vivo experiments on human. Finite Element Method supported by a C++ program was used to calculate the local SAR values, which represent the

biological effects of EM radiation. Local SAR values were calculated for two different head models; single and three-layered spherical models.

The application presented here seems to be reliable when comparing the results with the literature. But by this method, the calculation of the local SAR values is possible at the moment. This seems as a disadvantage of the method beside the advantage of calculation EM radiation with the problems having irregularly shaped boundaries because of the use of tetrahedral elements.

The pattern of energy absorption inside an irradiated body is non-uniform, and biological responses are dependent on distribution of energy and the body part that is affected. The rate of absorption and the distribution of EM energy in an organism depend on many factors: the dielectric composition (i.e., ability to conduct electricity) of the irradiated tissue, e.g., bones, with a lower water content, absorb less of the energy than muscles; the size of the object relative to the wavelength of the EMR (thus, the frequency); shape, geometry, and orientation of the object; and configuration of the radiation. The biological and health consequences of these exposure conditions need further investigation.

ACKNOWLEDGEMENTS

The work presented here was supported by Boğaziçi University Research Foundation Project No: 01HX102D.

REFERENCES

[1]Bernardi, P., S. Pisa, E. Pittorri, "Specific Absorption Rate and Temperature Increase in the Head of a Cellular-Phone User," *IEEE Transactions on Microwave Theory and Techniques*, Vol. 48, no. 7, pp. 1118-1126, July 2000.

[2]Guy, A.W., "Specific Absorption Rates of Energy in Man Models Exposed to Cellular UHF Mobile-Antennas Fields," *IEEE Transactions on Microwave Theory and Techniques*, Vol. MTT-34, no.6, pp.671-680, 1986.

[3]Nikita, K.S., G.S. Stamatakos, N.K. Uzunoğlu, and A. Karafotias, "Analysis of the Interaction Between a Layered Spherical Human Head Model and a Finite Length Dipole," *IEEE Transactions on Microwave Theory and Techniques*, Vol. 48, no.11, pp. 2003-2012, November 2000.

[4]Mangoud, M.A., R.A. Abd-Alhameed and P.S. Excell, "Simulation of Human Interaction with Mobile Telephones Using Hybrid Techniques Over Coupled Domains" *IEEE Transactions on Microwave Theory and Techniques*, Vol. 48, no.11, pp. 2014-2021, November 2000.

[5]Noyes, W.S., T.V McCaffrey, D.A. Fabry, M.S. Robinette, V.J. Suman, "Effects of Temperature Elevation on Rabbit Cochlear Function: Measured by Distortion-Product Otoacoustic Emission," Otolaryngology Head Neck Surgery, Vol. 115(6), pp.548-552, December 1996.

[6]Keck, W.J., Thorne, "Conduction of Thermal Stimuli in the Human Temporal Bone," Archives of Otolaryngology, Vol. 245(6), pp. 335-339, 1988.

[7]Gerald, C.F., P.O. Wheatley, *Applied Numerical Analysis*, Fifth Ed., California Polytechnic State University, Addison-Wesley Publishing Company, New York, 1998.

[8]Shapiro, A.R., R.F. Lutomirski, H. T. Yura, "Induced Fields and Heating Within a Cranial Structure Irradiated by an Electromagnetic Plane Wave," *IEEE Transactions on Microwave Theory and Techniques*, Vol. 19, no. 2, pp. 187-196, February 1971.

[9]Weil, C.M., "Absorption Characteristics of Multilayered Sphere Models Exposed to UHF/Microwave Radiation," *IEEE Transactions on Biomedical Engineering*, Vol.BME22, no. 6, pp. 468-476, November 1975.

[10]Stevens, N., and L.Martens, "Comparison of Averaging Procedures for SAR Distribution at 900 and 1800 MHz," IEEE Transactions on Microwave Theory and Techniques, Vol. 48, no.11, pp. 2180-2184, November 2000.

[11]Çelik, C.O., "EM Effects of Mobile Phones on Humanbeing," MS. Thesis, Boğaziçi University, Istanbul, Turkey, 2001.

EXHIBIT G

Spatial Distribution of High-Frequency Electromagnetic Energy in Human Head During MRI: Numerical Results and Measurements

Dina Šimunić,* Paul Wach, *Member, IEEE*, Werner Renhart, and Rudolf Stollberger

Abstract— Finite Element Method (FEM) using 26-node isoparametric finite elements was applied for modeling saddle-shaped head coils used in Magnetic Resonance Imaging (MRI) generating linearly polarized radiofrequency (RF) pulses at 64 MHz. The human head was modeled from MR scans of a volunteer and additional information were taken from *Atlas of Sectional Human Anatomy*. The physical dimensions of the head coil and the head permit a calculation of the outside magnetic field by a quasistatic approach. Of course, a full-wave approach was applied within the head. Values of specific energy—specific absorption (SA)—as well as of specific power—specific absorption rate (SAR)—were calculated by the method, simulating the real exposure conditions during MRI. Although the results of the used numerical method were compared previously to the results of the analytical solution with homogeneous sphere and to the results of RF measurements on heterogeneous phantom, a comparison between the numerical results of the modeled human head and *in vivo* measurements performed on the human head of the volunteer was made once more. Since the results are in excellent agreement, they argue for the correctness of the numerical method. The "worst-case" temperature deviations $\delta\theta$ of the "hot-spots" were calculated, as well. Finally, the results of SA, SAR, and $\delta\theta$ are compared to the existing recommendations.

I. Introduction

MEDICAL applications of electromagnetic fields, e.g., hyperthermia for cancer therapy or magnetic resonance imaging require an understanding of coupling electromagnetic fields to the human body. Although many numerical studies concerning hyperthermia based either on solving an integral equation (e.g., [1]) or using finite-difference time-domain [2] or finite element methods [3] exist, only few studies calculating heterogeneous realistic models of a human body in the field of magnetic resonance imaging, all using impedance method [4], [5] can be found. Magnetic resonance imaging (MRI) is a noninvasive medical diagnostic technique using different kinds of electromagnetic fields: a static magnetic field, a radiofrequency (RF) electromagnetic field and a switched gradient magnetic field. Since it has become a part of a standardized medical check-up, the interest in investigating possible adverse effects of MRI on human health has increased. High specific absorption rates (SAR) and concomitant "hot spots" may result due to the applied RF fields. On the contrary, switched gradient magnetic fields at low frequencies could cause neural and muscular stimulation. Since parts of the body such as the brain in the head are very sensitive to a change of the local temperature [6], the problems of induced current densities and energy deposition should therefore be treated in detail. Such an analysis can be given only by numerical methods, because analytical solutions using homogeneous cylinders or spheres can give only approximate values. For example it is shown in [9] and [10] that the highest power deposition occurs in the most distant parts from the center, but more detailed experimental work [11] and numerical calculations [4], [5] with a heterogeneous realistic structure of the human body give regions of high power depositions that are located in the interior parts.

TABLE I
Values of the Conductivity σ and Relative Permittivity ε_r of Tissues at 64 MHz Used in the Simulation

Tissue	σ(S/m)	ε_r
Bone	0.04	26
Cartilage	0.04	26
White Matter	0.4	70
Skin	0.73	73
Dura	0.73	73
Blood	1.15	80
Muscle	0.80	80
Nerve	0.47	90
Eye (Vitreous Humor)	1.9	100
Gray Matter	0.83	101
CSF	0.82	106

In order to find out the position of high energy deposition as well as their values, we performed finite element simulation for a heterogeneous model of the human head exposed to a linearly polarized RF magnetic field at 64 MHz. The case of modeling is established through the variable shape of the elements which do not have to be the same throughout. As with all finite element methods it is possible to zoom the area of interest (for instance in the case of a "hot spot") without increasing the number of elements. Obtained results from this calculation are valid for the exposure of a human head to continuous wave RF electromagnetic energy. Since MRI uses RF pulse sequence rather than continuous waves, we calculated specific absorption (SA)—absorbed energy per kg, as also done for

Manuscript received August 1, 1994; revised July 21, 1995. This work was supported by Austrian Bundesministerium für Wissenschaft, Forschung und Kunst, GZ 45268/2-46a/93. *Asterisk indicates corresponding author.*

*D. Šimunić is with the Graz University of Technology, Institute of Biomedical Engineering, Inffeldgasse 18, A-8010 Graz, Austria (e-mail: dina@ibmt.tu-graz.ac.at).

P. Wach is with the Graz University of Technology, Institute of Biomedical Engineering, Graz, Austria.

W. Renhart is with the Graz University of Technology, Institute for Fundamentals and Theory in Electrical Engineering, A-8010 Graz, Austria.

R. Stollberger is with the University of Graz, Center for Magnetic Resonance, A-8036 Graz, Austria.

Publisher Item Identifier S 0018-9294(96)00380-1.

0018-9294/96$05.00 © 1996 IEEE

Authorized licensed use limited to: Arizona Corporation. Downloaded on July 29, 2009 at 15:58 from IEEE Xplore. Restrictions apply.

electromagnetic pulse calculations in [12], Specific Absorption Rate (SAR) and the "worst case" temperature elevation $\delta\theta$ of the "hot spot."

Although the validity of the method was previously proven with the example of a homogeneous lossy dielectric sphere [6], in this paper the results of the calculation are compared to the in-vivo measurements performed by RF imaging–double pulse technique [7]. They show an excellent agreement.

Finally, the values of SA, SAR, and $\delta\theta$ calculated for the modeled human head are compared with the recommendations in the field [8], [22], [23].

II. Dielectric Properties of the Tissue

Recent papers [13], [14] use frequency-dependent properties of tissues for performing a numerical simulation in a broad frequency spectrum. Exciting magnetic RF pulses in the case of MRI can be considered as "narrow band" irradiation at 64 MHz. Therefore, as also indicated in [13], it seems that the first order Debye relaxation equation with well chosen relaxation frequency and values of the permittivity at "very low" and "very high" frequencies of the dispersion region can give sufficient approximation to the problem. Since in the literature the values of dielectric properties at 64 MHz were not found, the values of all the tissues in the head were interpolated at that frequency from the known values [18]–[20] in order to satisfy the mentioned Debye equation.

The complex conductivity σ^* used in the calculation is defined as follows

$$\sigma^* = \sigma + j\omega\varepsilon_0\varepsilon_r \tag{1}$$

where

- σ real part of the complex conductivity
- ω angular frequency $(2\pi f)$
- ε_0 permittivity of free space
- ε_r relative permittivity of the material

because, as shown in [6] such a definition enables inclusion of displacement current density, as well.

The values of σ and ε_r describing dielectric properties of various tissues are given in Table I.

III. The Finite Element Method

Although some finite element methods applied in the field of bioelectromagnetics use linear interpolation functions [3], our calculation uses higher order polynomials because such a formulation enables a much higher accuracy than the linear one [15], [16]. "Shape functions" are quadratic polynomials of the "serendipity family" for curvilinear second-order hexahedral elements. Also, the shape of isoparametric 3-D elements enables modeling with a much smaller number of elements for the same accuracy, which saves computing time and computer memory requirements. The isoparametric formulation defines a relationship between the element quantities at any point inside a finite element and the element nodal quantities by using the same interpolation functions for all the quantities. An isoparametric 3-D element with 26 nodes is depicted in Fig. 1.

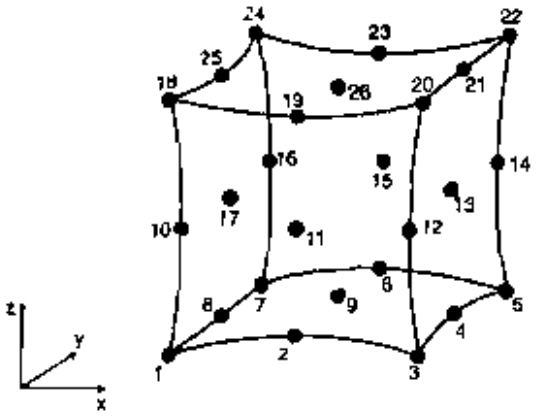

Fig. 1. Applied 26 noded isoparametric element in the global coordinate system.

The calculation of the field outside the head is performed assuming quasistatic conditions. This is possible because the wavelength at frequency 64 MHz (4.69 m) is much greater than the largest dimension of the exciting saddle shaped head coil (diameter and length are both 0.34 m). So, the magnetic field $\vec{H}_s$ of the coil is calculated by Biot–Savart's law

$$\vec{H}_s = \frac{I}{4\pi}\oint_{coil}\frac{d\vec{s}\times\nabla r}{r^2} \tag{2}$$

I denotes the coil current, $d\vec{s}$ a directed element of the coil and r the distance between a field point and a source point. The gradient ∇r is directed from the source point to the field point.

As described in [6] with the example of the lossy dielectric homogeneous sphere, the finite element formulation is based on the $\vec{A}$, V and Φ formulation. The vector magnetic potential ($\vec{A}$) and scalar electric potential (V) describe the fields in the model of a human head (conducting region) and in this region the following two differential equations have to be solved

$$\nabla\times\left(\frac{1}{\mu_0}\nabla\times\vec{A}\right)-\nabla\left(\frac{1}{\mu_0}\nabla\cdot\vec{A}\right)+\sigma^*(j\omega\vec{A}+\nabla V)=0 \tag{3}$$

$$\nabla\cdot(\sigma^*(j\omega\vec{A}+\nabla V))=0. \tag{4}$$

The total RF magnetic field strength $\vec{H}$ outside a dielectric object is defined as

$$\vec{H}=\vec{H}_s-\nabla\Phi. \tag{5}$$

The reduced scalar magnetic potential (Φ) and the undisturbed magnetic field strength $\vec{H}_s$ describe the field outside the object, so due to the vanishing divergence of magnetic induction ($\vec{B}$) the corresponding differential equation to be solved in the surrounding space is defined as follows:

$$\nabla\cdot(\mu_0\nabla\Phi)=\nabla\cdot(\mu_0\vec{H}_s). \tag{6}$$

The interface conditions—$\vec{H}$ tangential and $\vec{B}$ normal to be continuous—between the two regions ($\vec{A}$, V, and Φ) are enforced by evaluating a surface integral along this interface. Setting the normal component of $\vec{A}$ to zero at interfaces between the object and the surrounding space leads to the

Authorized licensed use limited to: Ansoft Corporation. Downloaded on July 29, 2009 at 15:58 from IEEE Xplore. Restrictions apply.

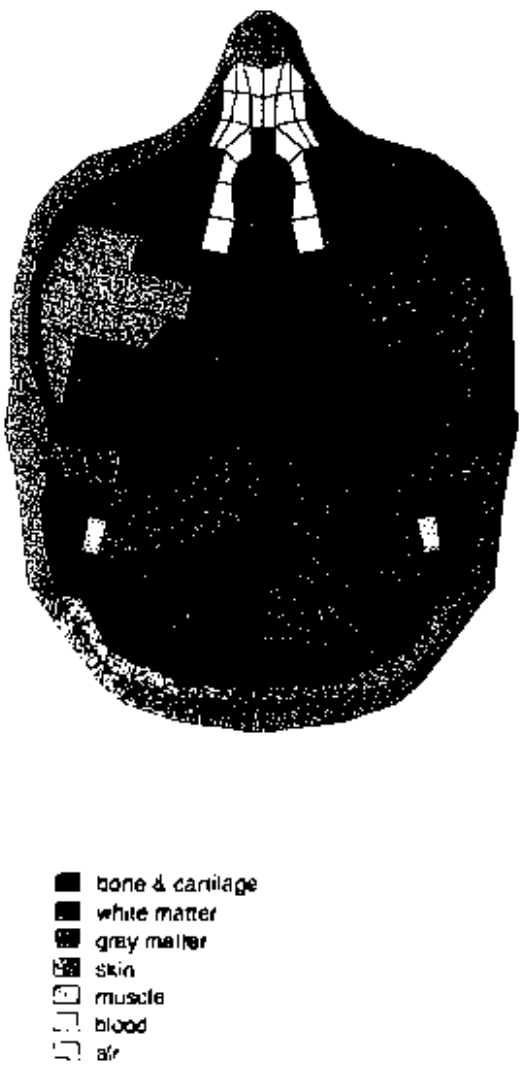

Fig. 2. Modeled slice no. 4/11 shown for illustration.

unique solution for the $\vec{A}$ when applying the Coulomb gauge, according to [6] and [17].

At farthest boundaries the reduced scalar magnetic potential Φ is set to zero [6].

IV. The Radio Frequency Imaging Method

Verification of the numerical calculations is performed by a special magnetic resonance imaging method [7]. This method utilizes the influence of the RF-field dependent flip angle $\alpha(\vec{x})$ of the magnetization on signal intensity $I(\vec{x})$. For amplitude modulated RF-pulses the flip angle distribution is proportional to the amplitude of the so-called "active" RF-field. In general, RF magnetic field $\vec{B}_1(\vec{x})$ can be decomposed in a longitudinal field $B_{1z}(\vec{x})$ and two counter rotating components $B_{1\sin}(\vec{x})$,

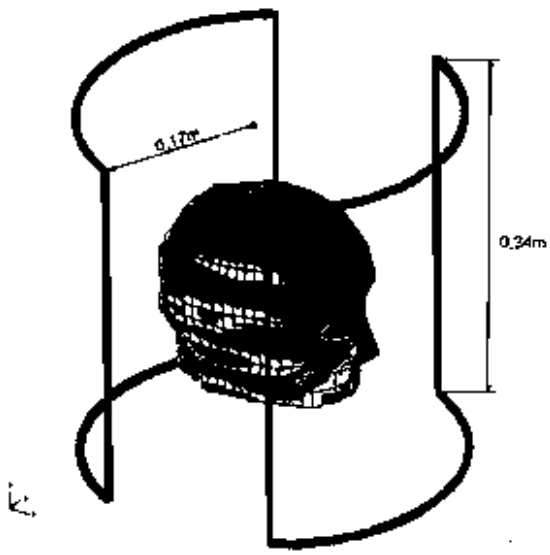

Fig. 3. Position of the modeled head in the saddle-shaped head coil of MRI.

$B_{1\cos}(\vec{x})$ of the transversal field $B_{1t}(\vec{x})$. The excitation of the magnetization is performed only by the "active" RF field, i.e., the circularly polarized transversal component $B_{1\sin}(\vec{x})$, which rotates in the same sense as spins precess.

In order to evaluate the RF-field dependent flip angle $\alpha(x)$ in an arbitrary object, one has to eliminate the additional position dependent influences on the signal intensity. These may result from the relaxation times $T_1(\vec{x})$, $T_2(\vec{x})$, the spin density $\rho(\vec{x})$ and the coil reception sensitivity $S(\vec{x})$. If two measurements are performed using the same scan parameters and a repetition time T_R greater than $5T_{1\,max}$, but two different excitation angles $\alpha_1(\vec{x})$ and $\alpha_2(\vec{x})$, the ratio of the signal intensity distributions $I_1(\vec{x})/I_2(\vec{x})$ gives the following equation

$$I_1(\vec{x})/I_2(\vec{x}) = \sin\alpha_1(\vec{x})/\sin\alpha_2(\vec{x}). \tag{7}$$

The function $I_1(\vec{x})/I_2(\vec{x})$ depends only on the flip angle distributions and $\alpha_1(\vec{x})$ and $\alpha_2(\vec{x})$. The additional condition $\alpha_2(\vec{x}) = 2\alpha_1(\vec{x})$ enables the calculation of the flip angle distribution $\alpha_1(\vec{x})$

$$\alpha_1(\vec{x}) = \arccos\left(\frac{1}{2}\cdot\frac{I_2(\vec{x})}{I_1(\vec{x})}\right). \tag{8}$$

The knowledge of an $\alpha_1(\vec{x})$ distribution makes it possible to determine the amplitude of the "active" B_1 field component by the following formula

$$B_{1\sin}(\vec{x}) = \frac{\alpha_1(\vec{x})}{\gamma\int_{-t_p/2}^{t_p/2} f(t)\,dt}, \tag{9}$$

where $f(t)$ is the modulating function, γ the gyromagnetic constant and t_p the pulse duration.

Authorized licensed use limited to: Ansoft Corporation. Downloaded on July 29, 2009 at 15:56 from IEEE Xplore. Restrictions apply.

TABLE II
THE CALCULATED SA DISTRIBUTION FOR THE 11 LAYERED MODEL OF THE HEAD FOR ONE 180° (ECHO) PULSE

Layer number	Max. SA [W/kg]	Region of max. SA	Max. SA in a "Hot Spot" [W/kg]	Region of a "Hot Spot"	Layer averaged SA
1.	0.20	blood vessel	0.19	blood vessel	0.02
2.	0.19	skin	0.18	muscle (jaw)	0.02
3.	0.20	skin	0.16	blood vessel	0.02
4	0.22	muscle (cheek bones)	0.12	muscle (cheek bones)	0.02
			0.17	blood vessel	
5	0.22	skin	–	–	0.02
6	0.22	skin	–	–	0.01
7	0.13	skin	0.10	CSF	0.01
8	0.12	skin	0.10	CSF	0.01
9.	0.12	skin	0.09	CSF	0.02
10.	0.10	skin	0.08	CSF	0.02
11.	0.10	skin	–	–	0.00

V. NUMERICAL MODEL OF A HEAD

Modeling the head followed significant changes in the anatomical structure with their different electric properties. The numerical head is modeled from MR scans of a volunteer. Nevertheless, the paramount reference was *Atlas of Sectional Human Anatomy* [24]. The model consists of 11 different tissues: skin, dura, white and gray matter, cerebrospinal fluid, nerve, eye (vitreous humour), blood, muscle, bone and cartilage. Applied isoparametric elements (Fig. 1) enable the description of the shape and internal structure with a reasonably low number of elements. The head model consists of 11 slices (with 1.5 cm distance). Each particular slice was partitioned into 296 elements (see Fig. 2). The shape of the elements is not the same and it follows the internal human head structure. One of the restrictions in the modeling refers to the condition that all the interior angles of the elements must be smaller than 180° to ensure the nonsingularity of the Jacobian operator relating the natural (global) coordinate derivatives to the local coordinate derivatives [15]. Satisfying the convergence criteria is only possible with complete and compatible, i.e., conforming elements. Due to the applied $\vec{A}$, V and Φ formulation and related boundary conditions (Φ is zero at the farthest boundaries), it was necessary to model two additional slices and the surrounding space. Since 3-D interpretation of the results is required, the same number of elements per slice is necessary for fulfilling the convergence and compatibility requirements [15].

The assumption of quasistatic conditions outside the head leads to the calculation of the exciting magnetic field on the interface between the two main areas (air-head) by Biot–Savart's law.

Assumed current in the coil is 0.27 A, which produces a value of magnetic field strength in the center of the coil of 21.49 A/m (27 μT). "Thermal equivalent" 180° rectangular pulse in a pulse sequence reaches this maximal value over a time period of 0.79 ms.

Summarizing, the model consists of 11 slices with 3256 elements with 11 different electrical properties, which can be, if necessary, further divided into finite elements for more detailed investigations. The whole model consists of 6420 elements (1164 elements are necessary for modeling farthest boundaries. They have dielectric properties of air). The model is shown in Fig. 3.

VI. RESULTS OF THE CALCULATION

Assuming the head as a homogeneous sphere and solving the Maxwell's equation for this case

$$\nabla \times \vec{E} = -\frac{\partial \vec{B}}{\partial t} \tag{10}$$

with constitutive relation ($\vec{J} = \sigma^* \cdot \vec{E}$) gives a dependence of the induced current density on the complex conductivity σ^*, operating frequency ω, radius of the object r and the amplitude of the high-frequency magnetic field. This very simplified calculation results in the highest current density in tissues most distant from the center of the head (e.g., skin). But in [9]–[11] the possibility of the presence of local heating due to the large local energy deposition inside highly heterogeneous structures is indicated. This statement is proven by numerical calculations [4], [5]. Although all these calculations and theories are made for a human torso, our results concerning human head, being also a highly heterogeneous structure, show some regions with high local rates of energy deposition, as well.

Table II gives maximum SA values, the position of these absolute maximum values in the layers, maximum SA's in the interior region of the layer (if any)—"hot spots," the position of these "hot spots" and the layer averaged SA's for each of the layers of the model. These values are calculated for one 180° (echo) pulse. The layer-averaged SA's are approximately 10 times lower than the maximum values for the various layers. It can be seen that according to theoretical predictions this region is mostly skin. But, results show also that energy distribution does not decrease continuously to the center—some regions inside the model show higher energy deposition, as well. In layer number 1, 3, and 4 these local increases of energy deposition are located in the position of blood vessels, in layer number 2 and 4 in muscles (in the neighborhood of bones—jaw and cheek bones) and in layers 7, 8, 9, and 10 in the cerebrospinal fluid (CSF).

On the basis of results presented in Table II, the values for the "worst case" can be calculated, i.e., how high is the

Authorized licensed use limited to: Aircraft Corporation. Downloaded on July 29, 2009 at 15:58 from IEEE Xplore. Restrictions apply.

TABLE III
THE CALCULATED SAR AND $\Delta\Theta_{tot}$ DISTRIBUTION FOR THE 11 LAYER MODEL OF THE HEAD FOR MULTISLICE TURBO SPIN-ECHO SEQUENCE

Layer number	Max SAR [W/kg]	$\Delta\Theta_{tot}$ in the region of max. SA (acc. to Table II) [°C]	Max. SAR in the "Hot Spot"	$\Delta\Theta_{tot}$ in the "Hot Spot" (acc. to Table II) [°C]	Layer averaged SAR [W/kg]
1.	3.28	0.31	3.15	0.31	0.35
2.	3.15	0.31	3.01	0.30	0.31
3.	3.41	0.33	2.61	0.25	0.34
4	3.67	0.36	3.67 2.89	0.36 0.27	0.31
5.	3.67	0.36	–	–	0.26
6	3.67	0.36	–	–	0.26
7.	2.10	0.21	1.38	0.14	0.24
8.	1.97	0.19	1.38	0.14	0.23
9.	1.97	0.19	1.44	0.15	0.23
10.	1.38	0.15	1.27	0.11	0.21
11	1.38	0.15	–	–	0.53

corresponding temperature elevation for the maximum value of the SA found in the numerical calculation for a head. This value is reached in the "hot spot" in the layer 4 for the region of the muscle and the cheek bones, because the highly conductive muscle tissue is just below low conductivity bone tissue. Here the SA reaches 0.22 J/kg.

The temperature increase $\delta\theta$ after one 180° (echo) pulse neglecting cooling effects is defined as

$$\Delta\Theta = \frac{1}{c}\mathrm{SA}|_{180^\circ\,max} \tag{11}$$

where c is specific heat of the medium [J/(kg°C)].

Using SA/180° max of 0.22 J/kg and c of muscle {3639 J/(kg °C)} [21], the temperature increase $\delta\theta$ is $6 \cdot 10^{-5}$ °C.

On the basis of performed calculation of transient temperature distribution for a "hot spot" (assuming a spherical shape with cooling properties of muscle [21] and a radius 0.5 cm embedded in a homogeneous medium), we neglect also the interpulse cooling effect during the echo spacing of 14 ms which leads to the worst case estimation. The total temperature increase of the "hot spot" is in this case

$$\Delta\Theta_{tot} = \Delta\Theta \cdot n_s \cdot n_p \tag{12}$$

where

n_s Number of imaged slices.

n_p Number of pulses for imaging one slice.

Considering the worst case of a typically used sequence—the multislice turbo spin-echo sequence with $n_s = 23$ and $n_p = 260$ $(16 \times 16 + 16/4)$ (i.e., one sequence for one slice contains sixteen 90° pulses carrying 1/4 of the power and $16 \times 16 = 256$ 180°(echo) pulses) gives $\Delta\Theta_{tot}$ of 0.36 °C.

Table III gives values of maximum SAR's averaged over six minutes for each slice, corresponding temperature increase, maximum SAR's in the interior regions ("hot spots"), the corresponding temperature increases and layer averaged SAR's. The duration of exposure to RF energy is taken to be 4.7 seconds (applied turbo multislice spin-echo sequence without averaging). The position of the maximum SAR in each layer, as well as the position of the maximum SAR in the interior region ("hot spot") are given in Table II.

The values for c [J/(kg °C)] used in table are taken from [21]—blood—3825, muscle—3639; skin—3662; CSF—that of water (20 °C)—4182. Existing recommendations in this field [8], [22], [23] take SA or SAR—depending on a duration time—as reference quantities for defining the restrictions on exposure. Since the exposure to RF fields in the case of the mentioned sequence lasts 4.7 sec. where the imaging time is only 1 minute and 32 seconds (less than 15 minutes), the recommended value of SAR is 4 W/kg averaged over any six minutes. From our calculation made for the specific modeled head and applied multislice turbo spin-echo sequence in the saddle-shaped head coil, the maximum SAR for a "hot spot" is 1.67 W/kg. Also, according to the same [8], [22], [23] the temperature elevation should not exceed 1 °C. This is also true in our calculation, not only for the whole head temperature increase, but also for the "hot spot."

The calculation was performed on DEC 3000—Model 500 AXP with 192 MBytes memory, 500 MBytes swapping space and 2.0 GByte external memory. The calculation of the whole head lasts 2100 sec. (35 minutes) of computer time.

VII. CONCLUSION

We have simulated the RF MRI exposure conditions for the human head by Finite Element Method using 26-noded isoparametric finite elements. The head has been modeled from MR scans of a volunteer with amended information from the *Atlas of Sectional Human Anatomy* [24]. The incident field has been calculated using quasistatic approach, because the physical dimensions of the RF MRI head-coil relative to the head permit it. The RF imaging method–Double pulse technique has been applied for a verification of the numerical method. Therefore the "active" magnetic field has been calculated and measured. As seen in Fig. 4(a) and (b), both results show very good agreement validating thereby the accuracy of the numerical method.

Magnetic resonance imaging uses RF pulse sequences in order to obtain images. In this paper a "worst" realistic

Authorized licensed use limited to: Artisoft Corporation. Downloaded on July 29, 2009 at 16:56 from IEEE Xplore. Restrictions apply.

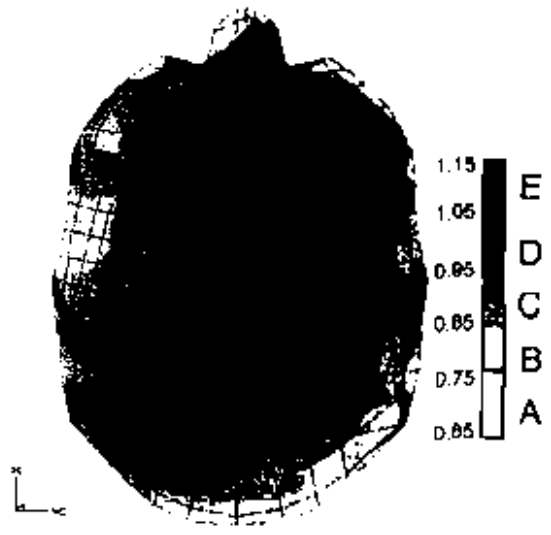

(a)

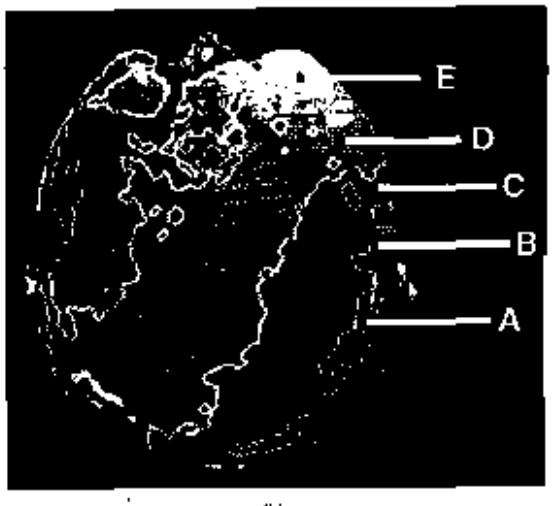

(b)

Fig. 4. (a) Calculated and (b) measured "active" component of the high-frequency field (64 MHz) in the human head (slice no. 5/11). N. B. The scales of Figs. 4(a) and 4(b) are identical (regions A–E), region A—0.65–0.75 (B1 normalized), region B—0.75–0.85, region C—0.85–0.95, region D—0.95–1.05 and region E—1.05–1.15.

sequence, turbo multislice spin-echo has been used for the calculations.

Using a realistic, inhomogeneous model of the human head we have shown that the SA, SAR distribution, and the maximum temperature increase ($\Delta\Theta_m$) of the "hot spot" for the 64 MHz (1.5 T static magnetic field) MRI's are within the safety guidelines [8], [22], [23]. Of course, our calculation concerns only the simulated case: the modeled head exposed to RF pulsed field (using multislice turbo spin-echo sequence) generated by saddle-shaped head coils. In [8] the restriction on maximum local tissue temperature in a head (38 °C), that should not be exceeded in any case, has been proposed. We find that the calculated worst case maximum temperature increase of 0.36 °C in the "hot spot" is considerably lower than the 1 °C—recommended increase of the whole body in NRPB safety guidelines.

Of course, the problem of possible stimulation effects due to the eddy currents in the human body caused by the switched gradients of the magnetic field still remains for investigation, as well as the calculation of RF energy deposition and temperature elevation at higher frequencies (due to higher static magnetic field) which will probably reach values closer to the limit values in the mentioned recommendations.

ACKNOWLEDGMENT

The authors benefited from the helpful comments and suggestions of O. P. Gandhi.

REFERENCES

[1] T. Deng, "Optimization of SAR distributions in liver and lung regions irradiated by the H-here annular phased array hyperthermia system," *IEEE Trans. Microwave Theory Tech.*, vol. MTT-39, pp. 852–856, May 1991.

[2] J.-Y. Chen and O. P. Gandhi, "Numerical simulation of annular-phased arrays of dipoles for hyperthermia of deep-seated tumors," *IEEE Trans. Biomed. Eng.*, vol. BME-39, pp. 209–216, Mar. 1992.

[3] K. D. Paulsen, X. Jia, and J. M. Sullivan Jr., "Finite element computations of specific absorption rates in anatomically conforming full-body models for hyperthermia treatment analysis," *IEEE Trans. Biomed. Eng.*, vol. BME-40, pp. 933–945, Sept. 1993.

[4] N. Orquil and O. P. Gandhi, "A 3-D impedance method to calculate power deposition in biological bodies subjected to time varying magnetic fields," *IEEE Trans. Biomed. Eng.*, vol. BME-35, pp. 577–583, Aug. 1988.

[5] M. Grandolfo, P. Vecchia, and O. P. Gandhi, "Calculation of rate of energy absorption by a human-torso model," *Bioelectromagnetics*, vol. 11, pp. 117–128, 1990.

[6] W. Renhart, C. A. Magele, K. R. Richter, P. Wach and R. Stollberger, "Application of eddy current formulations to magnetic resonance imaging," *IEEE Trans. on Magnetics*, vol. 28, no. 2, pp. 1517–1520, 1992.

[7] R. Stollberger, P. Wach, G. McKinnon, B. Justich, and F. Ebner, Book of abstracts (Works in Progress), p. 106, SMRM 1988.

[8] Documents of the NRPB, "Board statement on clinical magnetic resonance diagnostic procedures," vol. 2, no. 1, National Radiological Protection Board, Chilton, 1991.

[9] P. A. Bottomley and E. R. Andrew, "RF magnetic field penetration, phase shift and power dissipation in biological tissue: Implications for NMR imaging," *Phys. Med. Biol.*, vol. 23, no. 4, pp. 630–643, 1978.

[10] P. Bottomley, R. W. Redington, W. A. Edelstein, and J. F. Schenck, "Estimating radiofrequency power deposition in body NMR imaging," *Magnetic Resonance in Medicine*, vol. 2, pp. 336–349, 1985.

[11] P. Roschmann, "Radiofrequency penetration and absorption in the human body: Limitations to high-field whole-body nuclear magnetic resonance imaging," *Med. Phys.*, vol. 14, no. 6, pp. 922–931, 1987.

[12] J.-Y. Chen and O. P. Gandhi, "Currents induced in an anatomically based model of a human for exposure to vertically polarized electromagnetic pulses," *IEEE Trans. Microwave Theory Tech.*, vol. MTT-39, pp. 31–39, Jan. 1991.

[13] O. P. Gandhi, B.-Q. Gao, and J.-Y. Chen, "A frequency-dependent finite-difference time-domain formulation for induced current calculations in human beings," *Bioelectromagnetics*, vol. 13, pp. 543–555, 1992.

[14] D. M. Sullivan, "A frequency dependent FDTD method for biological applications," *IEEE Trans. Microwave Theory Tech.*, vol. MTT-40, pp. 532–539, Mar. 1992.

[15] M. V. K. Chari and P. P. Silvester (Eds.), *Finite Elements in Electrical and Magnetic Field Problems*, John Wiley & Sons, New York, 1980.

[16] O. C. Zienkiewicz, *The Finite Element Method in Engineering Science*. London: McGraw-Hill, 1971.

Authorized licensed use limited to: Ansoft Corporation. Downloaded on July 29, 2009 at 15:56 from IEEE Xplore. Restrictions apply.

[17] O. Biro and K. Preis, "On the use of the magnetic vector potential in the finite element analysis of three-dimensional eddy currents," *IEEE Trans. Magn.*, vol. 25, pp. 3145–3159, July 1989.
[18] H. P. Schwan, "Electrical properties measured with alternating current: Body tissues," in *Handbook of Biological Data* (Ed. Sandeen), Saunders, 1956.
[19] _____, "Electrical properties of tissue and cell suspension," in *Advances in Biological and Medical Physics*, pp. 147–209, 1957.
[20] M. A. Stuchly and S. S. Stuchly, "Dielectric properties of biological substances—Tabulated," *Journal of Microwave Power*, vol. 15, pp. 19–26, 1980.
[21] "Treatment planning and modeling in hyperthermia," A task group report of the European society for hyperthermic oncology, COMAC BME concerted action within the 4th Medical and health research programme of the European Commission, Postgraduate school of medical physics, II. University of Rome, 1992.
[22] F. D. A. "Magnetic resonance diagnostic device; panel recommendation and report on petitions for MR reclassification," *Federal Register*, vol. 53, pp. 7575–7579, 1988.
[23] S. G. Allen et al., "Proposals for basic restrictions for protection against occupational exposure to electromagnetic nonionizing radiations. Recommendations of an international working group set up under the auspices of the Commission of the European Communities," *Phys. Med.*, 1992.
[24] J. G. Koritke and H. Sick, *Atlas of sectional human anatomy*, Baltimore-Munich: Urban & Schwarzenberg, 1983.

Paul Wach (M-88) was born in Austria in 1940. He received his diploma and the Dr. Techn. degree in electrical engineering from Graz University of Technology in 1966 and 1967, respectively.

Since 1977 he has been a Professor and head of the Department for Biophysics at the Institute of Biomedical Engineering at Graz University of Technology. His main interest are general field theory, network theory, modeling, bioelectricity and biomagnetism.

Werner Renhart was born in Austria in 1959. He received the Dipl.-Ing. degree in electrical engineering in 1987 and the Dr. Techn. degree in 1990, both from the Graz University of Technology.

Until recently he has been with the Institute for Fundamentals and Theory in Electrical Engineering (IGTE) of the same university. His research is mainly on the finite-element computation of three dimensional eddy current fields.

Dina Simunić was born in Zagreb, Croatia. She received the Dipl.-Ing. degree in electrical engineering in 1983 and the M.S.E.E. in 1992, both from the University of Zagreb, Faculty of Electrical Engineering. In 1995 she received the Dr. Techn. degree from the Graz University of Technology. From 1993 she has been working on the project "Eddy currents in the human body during MRI" at Graz University of Technology, Austria. Her research interest are in the application of numerical methods in the bioelectromagnetics.

Dr. Simunić is the member of PIERS and BEMS, as well as the technical secretary of the project COST 244: "Biomedical Effects of Electromagnetic Fields."

Rudolf Stollberger received the Diploma degree in electrical engineering in 1984 and the Ph.D. degree in Technical Science in 1990 from Graz University of Technology.

From 1986 to 1987 he received an Erwin-Schrödinger-Foreign Scholarship at the department of Biomedical Engineering at the Swiss Federal Institute of Technology at Zurich. Since he has joined the Institute for Magnetic Resonance at the Karl-Franzens-University of Graz in 1987, he has been involved in the development and improvement of methods for magnetic resonance (MR) in medical diagnostics, the substitution of examination methods using ionizing radiation by MR procedures, image processing and multimodalities and the assessment of risks by locally enhanced radio frequency deposition.

Authorized licensed use limited to: Ansoft Corporation. Downloaded on July 29, 2009 at 15:26 from IEEE Xplore. Restrictions apply.